applied sciences

MDPI

Article

Parameter Identification Method of a Double-Layer Supercapacitor by Using a Real Voltage Source

Joaquín F. Pedrayes *, Enrique E. Zaldivar, María F. Quintana, Gonzalo A. Orcajo, Manés F. Cabanas and Juan C. Viera

Department Electrical Engineering, Universidad de Oviedo, 33204 Gijón, Spain; valdesenrique@uniovi.es (E.E.Z.); uo141648@uniovi.es (M.F.Q.); gonzalo@uniovi.es (G.A.O.); manes@uniovi.es (M.F.C.); viera@uniovi.es (J.C.V.)

* Correspondence: pedrayesjoaquin@uniovi.es

Abstract: This article presents a new method for obtaining the electrical parameters of a supercapacitor (SC) modeled as a constant resistor in series with a capacitance that linearly varies with its internal voltage. This model provides sufficiently accurate results when the SC is subjected to rapid, short-term charging and discharging. In other methods described in the literature, the parameters are obtained by charging or discharging the SC with a constant current source of high value. In this study, the electrical parameters are calculated by charging or discharging the cell with a real constant voltage source (RVS) or by discharging the SC through a known and constant resistance. The calculation procedure requires the measurement of the cell voltage as a function of time. Two alternative estimation methods have been employed: the three-point method (3PM) and the least squares method (LSM). A series of experimental tests were conducted on cells from various manufacturers, with capacitances ranging from 150 F to 600 F. The laboratory measurements were then compared with the results obtained from theoretical models incorporating the parameters obtained for the variable capacity model. The results demonstrated that this straightforward procedure is capable of accurately characterizing the main branch of any SC.

Keywords: electrical parameters estimation; model validation; supercapacitors; voltage source

check for updates

Citation: Pedrayes, J.F.; Zaldivar, E.E.; Quintana, M.F.; Orcajo, G.A.; Cabanas, M.F.; Viera, J.C. Parameter Identification Method of a Double-Layer Supercapacitor by Using a Real Voltage Source. *Appl. Sci.* **2024**, *14*, 9939. https://doi.org/10.3390/app14219939

Academic Editors: Haifeng Dai, Grzegorz Sierpiński, Dongdong Zhao and Bo Jiang

Received: 4 October 2024
Revised: 18 October 2024
Accepted: 28 October 2024
Published: 30 October 2024

1. Introduction

Supercapacitors (SCs) are energy storage devices used in many industrial applications due to their unique characteristics. These include their high specific power, which allows them to be charged and discharged very quickly. Their low internal resistance makes them to dissipate very little energy in the form of heat, which provides them with a high efficiency. Moreover, their useful life, under certain temperature conditions, can reach up to a million cycles, a value that is well above other storage systems, such as batteries, which makes them a good option in those applications that require a continuous exchange of energy. These devices have a wide operating temperature range, typically between −40 °C and 65 °C. Between 0 °C and 65 °C, their electrical parameters (resistance and capacitance) are quite stable and vary very little. In addition, at the end of their useful life, they can be easily recycled since they do not contain polluting or toxic chemical elements. The main component of porous membranes is carbon, an abundant material that is also compostable [1–7]. For all these reasons, these devices are a good option in many facilities.

In any industrial application where SCs are used it is essential to have a perfect understanding of their performance in different situations. Therefore, it is necessary to develop equivalent circuit models that combine simplicity and good accuracy. There are a multitude of SC models in the literature, which can essentially be divided into four categories [8]: electrochemical models, equivalent-circuit-based models, neural-network-based models, and fractional-order models. The final two groups, despite their ability to accurately reproduce the dynamic characteristics of SCs, do have some disadvantages. One such drawback is that they require a set of parameters that are not specified in the datasheets provided by manufacturers. In some cases, some of their variables do not even have a physical meaning and must be measured in laboratory tests using complex estimation algorithms. In addition, the accuracy they provide is rarely a necessary requirement for most industrial applications. This, together with their complexity, leads many researchers to opt for simpler solutions, even if they slightly penalize accuracy. In these cases, equivalent circuit models are usually chosen, as they can be used to obtain simple mathematical expressions for the different operating modes, producing results that, in the vast majority of cases, correctly characterize the real behavior of the SC. Moreover, these models can be employed in electrical circuit simulation environments.

The most common circuit-based models are shown in Figure 1. The first one (Figure 1a) is the constant capacitance RC series model. This representation of the SC is the most widely used due to its extreme simplicity and the existence of standardized test protocols, from which manufacturers provide its parameters in catalogs or datasheets. Moreover, it allows analytical expressions to be obtained for the four main operating modes: constant voltage charge/discharge, constant current, constant power [9–12], and constant resistance discharge, for both electrical and thermal analyses [13–16]. For the aforementioned reasons and because its results are more than acceptable, it is mostly used in the sizing of SC banks [17–22]. In studies of self-discharge, a leakage resistor (R_L) is connected in parallel with the capacitance. However, in the majority of other studies, this is typically considered to be negligible, given that its ohmic value is very high, and therefore, the current flowing through it is very low. Although many researchers consider R_L to be constant, H. Yang et al. [23] have treated it as a variable resistance dependent on the internal voltage. However, there are no mathematical expressions that allow its analytical function to be determined by laboratory testing.

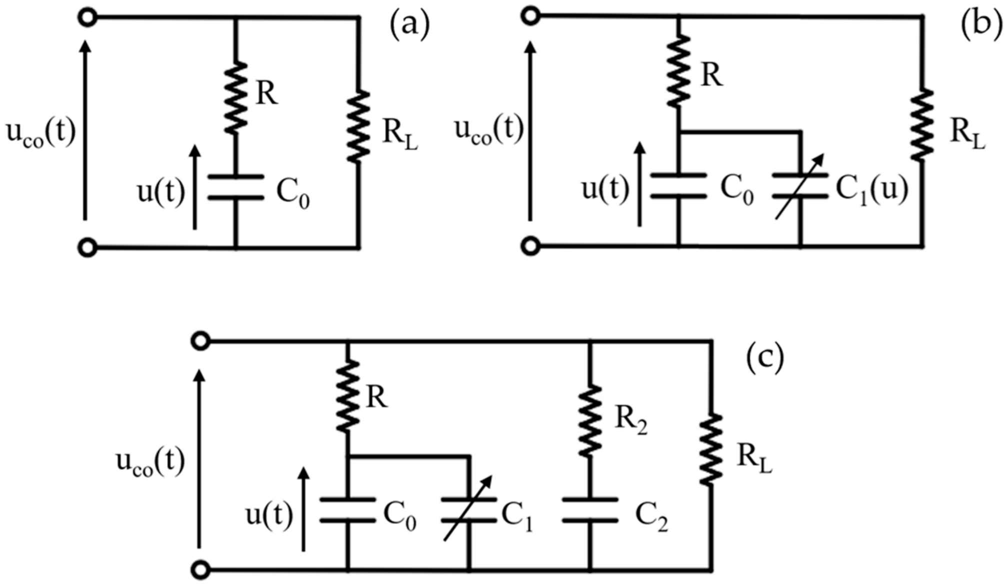

Figure 1. *Cont.*

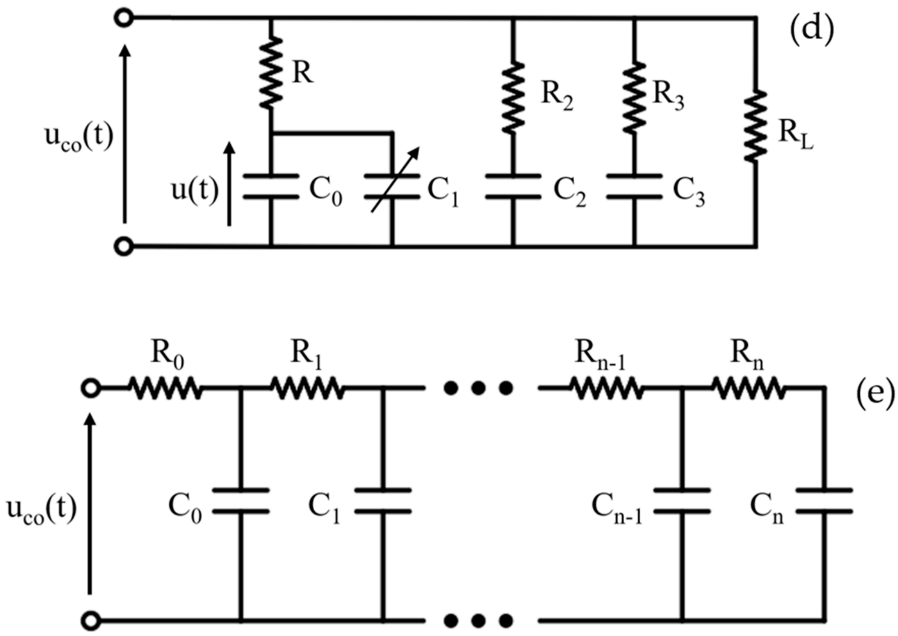

Figure 1. Some of the most widely used RC circuit-based SC models.

A more sophisticated SC model than the previous one is depicted in Figure 1b, where the capacitance is not constant but varies linearly with the internal voltage [24–27]. This model accurately emulates the behavior of the SC when it is rapidly charged or discharged (short-term characterization), but its accuracy may be insufficient to analyze the cell response when it is charged or discharged slowly (medium- or long-term characterization), due to the charge redistribution phenomena that occur inside the SC [28]. To enhance the precision of this model, additional RC branches are frequently connected in parallel, typically of constant capacity, with time constants that are considerably larger than those of the primary branch [29–31]. Two-branch (Figure 1c) or three-branch (Figure 1d) models can be employed, and even more branches can be added. As in the constant capacitance model, the leakage resistance, R_L, can be included if self-discharge requires to be analyzed. The models with two or more branches, despite their ability to accurately simulate the behavior of the SC in all situations, present a disadvantage in that they are complex to express mathematically in terms of the main operating variables, such as current and voltage. Consequently, these models are often considered using electrical circuit simulation software.

Other models that accurately reproduce the dynamic behavior of SCs are transmission line models (Figure 1e). However, working with them requires numerical simulation tools applied to a model carefully adjusted to the characteristics of the cell. Unfortunately, this adjustment, which involves measuring all the components using complex estimation methods, limits their use to very specific studies. In fact, the high accuracy provided by these models is rarely needed in industrial applications.

Among the models based on electrical circuits that have been presented by other researchers, two are particularly suitable to be used in most industrial applications, combining simplicity and good accuracy. The one-branch variable-capacity model (Figure 1b) is valid for the study of short-term behavior, while the two-branch model shown in Figure 1c is suitable for characterizing the behavior from short-term to medium- to long-term operation. Both models do not require the calculation of many components, as in more complex approaches, and provide sufficiently accurate results for most studies requiring the analysis of SCs. However, manufacturers do not provide the values of all the parameters of these models, so estimation procedures from laboratory tests have been developed in previous studies. These methods typically use charging or discharging the cell with a very high constant current source.

The main operating modes of SCs can be summarized as follows: constant current charge/discharge, constant power, constant voltage real source, or constant resistance discharge. Although the first two are widely used, the latter also appear in many industrial applications. For example, when charging an SC, it is common to do so in two stages. The first one is carried out at a constant current of a high value. To avoid damaging the SC, the external voltage of the cell is controlled. When the rated value of the cell is reached externally, U_N, the internal voltage will not yet have reached this rated voltage due to the voltage drop across its series resistor, so the cell will not be 100% charged [32]. Therefore, in the second phase, the charge is completed using a real constant voltage source, whose no-load voltage is equal to U_N. In this way, full charge is achieved with high efficiency and in a relatively short time. This method is known as the constant-current, constant voltage method (CC/CV) [33–35].

Recent works have explored the possibility of installing SCs on solar panels, so that they have their own built-in energy storage system. This can be very useful in stand-alone systems, uninterruptible power supplies, or emergency lighting. In these cases, the SCs are usually connected directly to the solar panel, which will work, in almost all the range of voltages, as a real constant voltage or current source, both of which can be reduced to the first case [36–38].

SCs are also used to absorb transient surge voltages of several kV, but of short duration, where the energy involved is low, in an application known as SCASA (Supercapacitor Assistant Surge Absorb). Although SCs have low internal resistance, because their capacitance is very high, their time constant is high enough to withstand the transient surge voltages that occur in the grid, whose durations are usually in the order of milliseconds. To analyze their ability to absorb these surges, SCs are subjected to high-voltage pulses, generated with a constant and very high voltage source, but of short duration [39–42].

There are industrial applications where SCs work as a power supply for resistive heaters. N. Kularatna et al. [43,44] have proposed a system for heating water in domestic installations, where the SCs discharge their energy on resistors. These are usually made of nichrome, a material whose resistivity varies only slightly with temperature. As the heat generated in them will be transmitted directly to the water, their ohmic value will hardly increase. A similar idea is used by D. S. Chavan et al. [45] to avoid ice accumulation on wind turbine blades, which can affect their aerodynamic performance. In the manufacturing process, a nichrome coil is embedded along the entire length of the blade, which receives current pulses every minute generated by an SC that discharges its energy on these filaments, which act as heaters. In both cases, it is considered that the SCs are discharged rapidly over practically constant resistances. The main disadvantage of this technique is that it is necessary to charge the SC many times, since its stored energy is low, and in addition, it must be delivered very quickly, so the SC is discharged very fast. However, this system has a very high efficiency since the resistance used as a heater will be quite larger than the internal resistance of the SC, so almost all the energy discharged by the SC will be transformed into heat in the heating resistor. In addition, since the SC withstands a high number of charge and discharge cycles, it will make the set very durable.

The main interest in estimating the values of the electrical parameters of a cell is to find out its aging level. According to the manufacturers, when a cell reaches the end of its useful life, it will show a decrease in its capacity (typically 20–30%) compared to what it had at the beginning, while the internal resistance increases by 100%. To know how far a cell is from reaching its end, it is necessary to make periodic monitoring of these parameters. When they reach values close to the limit thresholds, the cells must be replaced with new ones, before an unexpected failure occurs that could affect the entire system where they are installed. This monitoring will be part of the system's predictive maintenance.

This study proposes an alternative method for the calculation of the variable capacitance main branch parameters (R, C_0, and k_c) by rapidly charging or discharging the SC with a real voltage source or by discharging the cell with a constant resistance, which can be used by taking advantage of any of the industrial applications mentioned previously. This new method makes the necessary test equipment simple and economical, especially when discharging on a constant resistance. The values of the external voltage, $u_{co}(t)$, measured during the charging or discharging of the SC, will be taken as the starting data. These will be employed considering the model depicted in Figure 1b. In the event that the parameters of the second branch (Figure 1c) are also to be obtained, since it is necessary to calculate the parameters of the first branch beforehand, the newly developed algorithm will also be very useful.

The paper is arranged as follows: Section 2 will show the mathematical study to obtain the electrical variables of an SC connected to a voltage source, valid for both charging and discharging. Section 3 describes two methods for obtaining the equivalent circuit parameters. In Section 4, several tests are carried out with cells of different capacitances and from different manufacturers, on which the methods described in the previous section have been verified. Finally, the study finishes with a section on conclusions.

2. Materials

2.1. Variable Capacitance Model

The short-term branch, as depicted in Figure 1b, comprises a resistor, R, of a constant value, connected in series with a capacitance that varies linearly with the internal voltage, u, according to the following expression:

$$C(u) = C_0 + C_1(u) = C_0 + k_c \cdot u. \quad (1)$$

The capacitance of the SC, C(u), is equivalent to the parallel association of two others. The first is a constant value, C_0, which is known as the Initial Capacitance. This is the value presented by the SC when it is completely discharged. The second one is $C_1(u)$, which represents the variable part and grows linearly with the internal voltage. The slope of the linear function C(u), k_c, is measured in [F/V]. The rated capacitance, C_N, provided by the manufacturers, is the capacitance of the SC when it is charged up to its rated voltage, U_N, and exhibits the following value:

$$C_N = C_0 + k_c \cdot U_N. \quad (2)$$

The capacity C(u) can be expressed as a function of the rated capacity, C_N, and the rated voltage, U_N, as follows:

$$C(u) = C_0 + \frac{C_N}{U_N} \cdot \left(1 - \frac{C_0}{C_N}\right) \cdot u = C_N \cdot k_0 + \frac{C_N}{U_N} \cdot (1 - k_0) \cdot u. \quad (3)$$

The k_0 value, designated as the Normalized Initial Capacitance, is the quotient between the Initial Capacitance, C_0, and the rated capacitance, C_N. This variable typically ranges between 0.6 and 0.85 in most families of SCs [46]. In the one-branch model (Figure 1b), three parameters must be obtained: R, C_0, and k_c. Although all three components are known to vary slightly with temperature, if the SC is operating between 20 °C and 65 °C, the variations they undergo can be considered negligible [47,48]. Significant changes in the resistance R occur only below 0 °C, which increases as the viscosity of the electrolyte increases (the capacitance decreases very slightly); therefore, the influence of temperature will not be considered in this study. The proposed method is valid for the determination of the cell parameters at any operating temperature. Over the brief duration of the test, the temperature of the SC will remain constant or will present small variations that are considered negligible.

In the calculation of the variables of the first branch of the SC, it can be assumed that all the current injected during fast charging will flow into the variable capacitance of the first branch. The secondary branch (R_2, C_2–Figure 1c) will have a negligible influence because its dynamics are much slower, given that it presents a much larger time constant ($R \cdot C_N << R_2 \cdot C_2$). While the voltage in the first branch rises rapidly, it hardly increases in the secondary branch. Once the charging current is canceled, part of the charge stored in the first branch will be slowly redistributed to the second branch, in a new transient state, until the voltages of the capacities of both branches are equalized. It will therefore be considered that, during fast charging, the secondary branch can be neglected [49–51].

2.2. Test Bench

In this novel procedure, the SC will be connected to a real constant voltage source, whose no-load voltage, E, and its internal resistance, R_c, are known (Figure 2). The internal voltage of the SC, which defines the energy stored in it, will be designated by u(t), while the external voltage, $u_{co}(t)$, will be measured at its terminals. The initial internal voltage of the SC, u (t = 0), will be denoted as U_0.

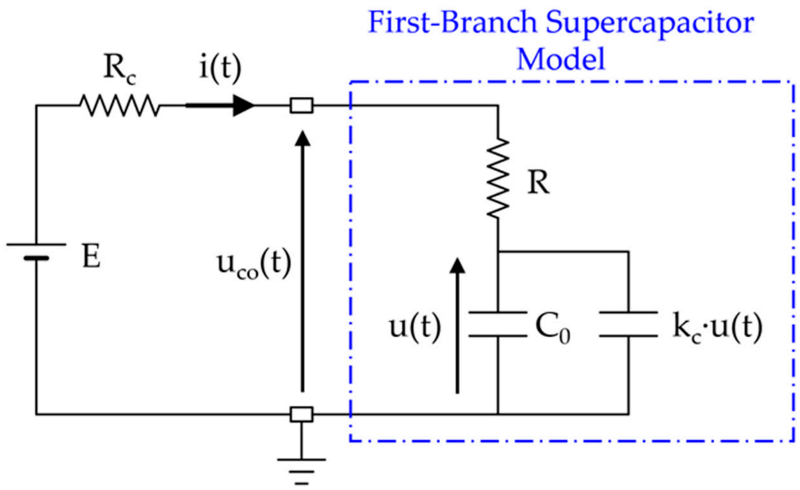

Figure 2. Schematic diagram of the connection between the SC and the RVS.

The equations presented in this article are valid for both the charging and discharging modes of the SC. The method is also valid if a constant value resistor R_c is used instead of a real voltage source, since this would be a "particular" voltage source where E = 0 V. To present the most comprehensive and general results possible in the cases studied below, a charging process will be used in the whole study. It is not necessary to utilize high-performance instrumentation to apply the method proposed in this paper. A low-cost data acquisition card or an oscilloscope with waveform storage capability may be employed to measure the evolution of the external voltage, $u_{co}(t)$, as a function of time. If the voltage source presents a reduced capacity to deliver current, a limiting resistor, R_{lim}, can be series connected with the SC. This will result in the resistance R_c that will appear in the equations being the sum of the internal resistance of the real voltage source plus the limiting resistor and the resistances of the cables used to connect all the elements.

2.3. Electrical Analysis of an SC Connected to an RVS

When an SC modeled with the main branch only is connected to a real constant voltage source (E, R_c), a time function, g(t), measured in volts, can be defined, as demonstrated in [31], whose expression is as follows:

$$g(t) = \frac{1}{k_m} \cdot W_0\left(k_p \cdot \exp(-k_n \cdot t)\right). \tag{4}$$

The function $W_0(x)$ is the main or upper branch of the Lambert-W function [52,53]. The constants k_m [V^{-1}], k_n [s^{-1}], and k_p (dimensionless) depend on the variables of the main branch (C_0, k_c, and R), those of the real voltage source (E, R_c), and the initial internal voltage of the SC, U_0, as shown in the following expressions:

$$k_m = \frac{2 \cdot k_c}{C_0 + 2 \cdot k_c \cdot E}. \quad (5)$$

$$k_n = \frac{1}{(R_c + R) \cdot (C_0 + 2 \cdot k_c \cdot E)}. \quad (6)$$

$$k_p = k_m \cdot (U_0 - E) \cdot \exp(k_m \cdot (U_0 - E)). \quad (7)$$

In (7), exp(x) represents the exponential function. The variable g(t), as defined in (4), presents a positive sign when the SC is discharging on the RVS ($U_0 > E$) and a negative sign otherwise ($U_0 < E$). The instantaneous values of the internal voltage, u(t), the discharge current, i(t), and the external voltage of the cell, $u_{co}(t)$, can be obtained from the following equations, which are derived from the function g(t) [31]:

$$u(t) = E + g(t). \quad (8)$$

$$i(t) = \frac{g(t)}{R_c + R}. \quad (9)$$

$$u_{co}(t) = E + \left(\frac{R_c}{R_c + R} \right) \cdot g(t). \quad (10)$$

The function g(t) can be defined as the difference between the internal voltage of the SC, u(t), and the no-load voltage of the RVS, E. It is also possible to calculate the time that must elapse for the variable g(t) to reach a specific value, given an initial value $g_0 = U_0 - E$. This time, t, presents the following value:

$$t = 2 \cdot k_c \cdot (R_c + R) \cdot \left[\left(\frac{C_0}{2 \cdot k_c} + E \right) \cdot \log \left(\frac{U_0 - E}{g} \right) + U_0 - E - g \right]. \quad (11)$$

In (11), log(x) represents the Neperian or natural logarithm of x. To simplify the expressions that will be part of the final solution, the following constants are defined:

$$k_1 = \frac{C_0}{2 \cdot k_c} + E. \quad (12)$$

$$k_2 = 1 + \frac{R}{R_c}. \quad (13)$$

$$k_3 = \frac{1}{2 \cdot k_c \cdot (R_c + R)}. \quad (14)$$

The first constant, k_1, is measured in units of voltage [V], the second, k_2, is dimensionless, and the third, k_3, is measured in [$V \cdot s^{-1}$]. The functions u(g) and $u_{co}(g)$, derived from (8) and (10), respectively, facilitate the straightforward determination of g(u) and $g(u_{co})$. By composing these functions with t(g), as presented in (11), the time required for the internal and external voltage to reach a specified value can be calculated, thereby obtaining the functions t(u) and $t(u_{co})$. The function $t(u_{co})$ will be employed to compute the three parameters of interest. The final expression, as a function of the constants k_1, k_2, and k_3, is as follows:

$$t = \frac{1}{k_3} \cdot \left[k_1 \cdot \log \left(\frac{U_0 - E}{k_2 \cdot (u_{co} - E)} \right) + U_0 + \frac{R}{R_c} \cdot E - k_2 \cdot u_{co} \right]. \quad (15)$$

3. Methods

This section will present two methods for obtaining the main branch parameters from the cell terminal voltage, $u_{co}(t)$, while charging or discharging through an RVS.

3.1. Three-Point Method (3PM)

The external voltage as a function of time during cell charging will produce a curve like that shown in Figure 3. Three measurements will be taken at sufficiently distant points in time, whose values will be $P_1 = (0, u_{co1})$, $P_2 = (t_2, u_{co2})$, and $P_3 = (t_3, u_{co3})$. It is assumed that the initial sample will be collected at $t_1 = 0$ s. If the value of the voltage source, E, is added to both members of the function $t(u_{co})$ presented in (15), the relationship between the time t and the external voltage u_{co} is expressed as follows:

$$k_3 \cdot t + E = k_1 \cdot \log\left(\frac{U_0 - E}{k_2 \cdot (u_{co} - E)}\right) + U_0 + k_2 \cdot (E - u_{co}). \quad (16)$$

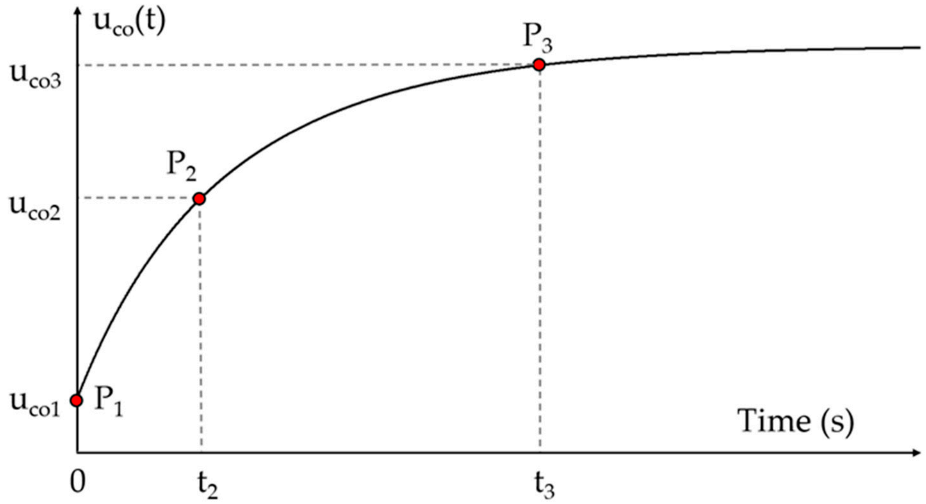

Figure 3. External voltage as a function of time, with three sufficiently spaced samples to be chosen.

The value of R can be calculated from the first value of the external voltage, u_{co1}. At time t = 0, this voltage is given by:

$$u_{co1} = \frac{R_c \cdot U_0 + R \cdot E}{R + R_c}. \quad (17)$$

From (17), the value of R is directly calculated as follows:

$$R = \left(\frac{u_{co1} - U_0}{E - u_{co1}}\right) \cdot R_c. \quad (18)$$

Once the value of R has been obtained, the value of the constant k_2 can be calculated using Equation (13). The two remaining measurements, corresponding to the points P_2 and P_3, can then be combined into a system of equations, where the value of k_2 is already known:

$$\begin{cases} k_3 \cdot t_2 + E = k_1 \cdot \log\left(\frac{U_0 - E}{k_2 \cdot (u_{co2} - E)}\right) + U_0 + k_2 \cdot (E - u_{co2}) \\ k_3 \cdot t_3 + E = k_1 \cdot \log\left(\frac{U_0 - E}{k_2 \cdot (u_{co3} - E)}\right) + U_0 + k_2 \cdot (E - u_{co3}) \end{cases}. \quad (19)$$

Solving this system of equations yields the values of the constants k_1 and k_3:

$$k_1 = \frac{E - U_0 + k_2 \cdot \left(\left(\frac{t_2}{t_3 - t_2}\right) \cdot (u_{co2} - u_{co3}) + u_{co2} - E\right)}{\log\left(\left(\frac{U_0 - E}{k_2 \cdot (u_{co2} - E)}\right) \cdot \left(\frac{u_{co3} - E}{u_{co2} - E}\right)^{\frac{t_2}{t_3 - t_2}}\right)}. \quad (20)$$

$$k_3 = \frac{k_1 \cdot \log\left(\frac{u_{co2} - E}{u_{co3} - E}\right) + k_2 \cdot (u_{co2} - u_{co3})}{t_3 - t_2}. \quad (21)$$

Once the three constants, k_1, k_2, and k_3, are known, it is straightforward to obtain C_0 and k_c values from the expressions (12) and (14):

$$k_c = \frac{1}{2 \cdot R_c \cdot k_2 \cdot k_3}. \quad (22)$$

$$C_0 = \frac{k_1 - E}{R_c \cdot k_2 \cdot k_3}. \quad (23)$$

The proposed method is straightforward, requiring only three measurements of the function $u_{co}(t)$ to obtain the desired parameters. When the three external voltage measurements (u_{co1}, u_{co2}, and u_{co3}) are acquired, they may have oscillations with respect to the real value due to the errors that occur when using a data acquisition system, e.g., due to the resolution of the A/D converter. If a low sampling period has been used when measuring the voltage $u_{co}(t)$, instead of only using the three-point measurements, u_{coi}, one or two more measurements can be taken around each sample, above and below that value, and then averaged between them. This compensates for the error that may occur with a single measurement.

Another way to estimate the three parameters of the main branch is by using a mathematical procedure that utilizes the complete recording of the external voltage to identify the values of R, C_0, and k_c, which provide the best fit between the theoretically calculated external voltage and the measured voltage. One suitable approach is the least squares method, as it enables the errors that arise when measuring the series of values of the function $u_{co}(t)$ to be compensated. By using a real voltage source, this method can be applied in a single step, as $u_{co}(t)$ can be expressed as a function of the three constants to determine the time, the RVS values, and the initial internal voltage of the SC, obviating the necessity to know other functions such as the circuit current and the instantaneous internal voltage of the SC or its derivative. In addition, the SC need not be initially discharged but can have any initial internal voltage U_0.

3.2. Least Squares Method (LSM) Using the External Voltage, $u_{co}(t)$

As mentioned above, this section will present the application of the least squares method using the entire time series of $u_{co}(t)$. During the acquisition of the signal, two vectors will be obtained; the first formed by the times elapsed from the beginning to the end of the measurement, t_i, with i = 1, 2, . . ., n, and the second with the values reached by the external voltage, u_{coi}, for each time instant t_i. One of the advantages of this procedure is that it does not require the use of a high sampling frequency, which reduces the cost of the necessary instrumentation. To apply the calculation method, U_0, E, R_c, and the expression of the time, t, when u_{co} would reach a certain value, that is, the function $t(u_{co})$ obtained in Equation (15), are available. This function can be expressed in a more compact form as follows:

$$t = \alpha + \beta \cdot \log(u_{co} - E) + \gamma \cdot u_{co}. \quad (24)$$

To abbreviate the above expression, the constants α, β, and γ will be defined. The first two are measured in [s], while the third is measured in [$s \cdot V^{-1}$]. These constants can be expressed as a function of k_1, k_2, and k_3, which in turn depends on the three parameters to determinate, R, C_0, and k_c, on the variables of the RVS (E, R_c) and the initial cell voltage, U_0. Their values are as follows:

$$\alpha = \frac{1}{k_3} \cdot \left[k_1 \cdot \log\left(\frac{U_0 - E}{k_2} \right) + U_0 + \frac{R}{R_c} \cdot E \right]. \quad (25)$$

$$\beta = -\frac{k_1}{k_3}. \quad (26)$$

$$\gamma = -\frac{k_2}{k_3}. \quad (27)$$

Subsequently, function F, which represents the sum of the squares of the differences between the measured time instants, t_i, and the estimated times from (24), will be defined. The function F is expressed as follows:

$$F = \sum_{i=1}^{n} \left(t_i - \alpha - \beta \cdot \log(u_{coi} - E) - \gamma \cdot u_{coi}\right)^2. \tag{28}$$

The objective now is to calculate the constants α, β, and γ that make the value F minimum. To do so, the latter will be derived with respect to each of these three parameters, and each derivative will be equal to zero. The resulting system, expressed in matrix form, is the following:

$$\begin{bmatrix} \sum_{i=1}^{n} t_i \\ \sum_{i=1}^{n} t_i \cdot \log(u_{coi} - E) \\ \sum_{i=1}^{n} t_i \cdot u_{coi} \end{bmatrix} = [M] \cdot \begin{bmatrix} \alpha \\ \beta \\ \gamma \end{bmatrix} = \begin{bmatrix} a_{11} & a_{12} & a_{13} \\ a_{21} & a_{22} & a_{23} \\ a_{31} & a_{32} & a_{33} \end{bmatrix} \cdot \begin{bmatrix} \alpha \\ \beta \\ \gamma \end{bmatrix}. \tag{29}$$

The matrix [M] is symmetric and its determinant is nonzero. The coefficient a_{11} represents the total number of samples, n, taken from the function $u_{co}(t)$. The remaining elements of the matrix are as follows:

$$a_{22} = \sum_{i=1}^{n} \left(\log(u_{coi} - E)\right)^2. \tag{30}$$

$$a_{33} = \sum_{i=1}^{n} {u_{coi}}^2. \tag{31}$$

$$a_{12} = a_{21} = \sum_{i=1}^{n} \log(u_{coi} - E). \tag{32}$$

$$a_{13} = a_{31} = \sum_{i=1}^{n} u_{coi}. \tag{33}$$

$$a_{23} = a_{32} = \sum_{i=1}^{n} u_{coi} \cdot \log(u_{coi} - E). \tag{34}$$

Solving the equations system (29) yields the constants α, β, and γ. Once these are known, along with the values of k_1, k_2, and k_3, as defined in Equations (12)–(14), respectively, the parameters of the main branch of the SC can be obtained. The value of R is first calculated, and its final expression, after some operations, is as follows:

$$R = \frac{\gamma}{\beta} \cdot \frac{R_c \cdot (U_0 - E)}{W_0\left(\frac{\gamma}{\beta} \cdot \exp\left(-\frac{1}{\beta} \cdot (\alpha + \gamma \cdot E)\right)\right)} - R_c. \tag{35}$$

Once the value of R has been obtained, the values of C_0 and k_c are obtained by using the following formulas:

$$k_c = \frac{-\gamma \cdot R_c}{2 \cdot (R_c + R)^2}. \tag{36}$$

$$C_0 = \frac{-\beta}{(R_c + R)} - 2 \cdot k_c \cdot E. \tag{37}$$

For this method to yield accurate results, the charging or discharging process must be completed in a relatively short period of time. This is necessary to prevent the slower dynamics of the secondary branch of the SC from influencing the primary branch. Therefore, it is advisable to use a real voltage source with a low internal resistance R_c. The voltage of this source may be higher than the rated voltage of the SC, provided that the charging is stopped before the SC exceeds its rated value. If it is not desired that the source initially injects a too high a current, it is sufficient to connect a resistor of a known value in series with the SC to limit it. This avoids the possibility of damaging the voltage source. However, it is necessary to find a commitment between the current limitation and the charging time, as the latter should not be slowed down too much. If the tested SC has a low-rated capacitance and during the test, it is observed that it has reached the steady state, a shorter charging time must be taken to ensure that the first branch is far from reaching the value of the voltage source E. This method is applicable to both a charge ($E > U_0$) and a discharge ($E < U_0$), as well as to a discharge through a constant resistance ($E = 0$).

The 3PM method has the advantage that it only needs three measurements of the voltage $u_{co}(t)$ and the three parameters are very easily obtained using simple mathematical functions. The LSM method is more accurate, as it estimates the three parameters using the whole register of $u_{co}(t)$, thus getting the best fit, but for the calculation of the resistance, it is necessary to use the Lambert-W function.

The two methods described have the following advantages over other methods in which an ideal current source is used to carry out the charging or discharging:

1. These methods can be used directly in those applications where the SC is to operate connected to an RVS or be discharged through a constant resistance, which makes it possible to estimate the parameters during normal operation of the SC.
2. Only the cell terminal voltage, $u_{co}(t)$, needs to be measured. It is not necessary to obtain any other signal, such as the internal voltage or any of its derivatives, nor is it necessary to adjust those functions by means of polynomials or Taylor series, as is performed in other methods [30], which adds complexity and may cause additional errors.
3. The three parameters (R, C_0, and k_c) can be obtained directly by both methods (3PM and LSM) in a single step. However, in other approaches, like the one proposed by Sergio M. Coca et al. [30], C_0 and k_c values must be obtained in the first stage using a discharge of SC with a high constant current. From this, in the second phase, the value of the resistance R.
4. When an ideal constant current source is used, a high value of current is required to measure the voltage drop across the internal resistance, $\Delta V = R \cdot I$. For example, Faranda [28] used 33 A current source to estimate the parameters of a 600 F cell. It must be considered that the higher the capacitance of an SC, the lower its internal resistance R. Sergio M. Coca et al. [30] used 120 A discharge current in their method for a 3000 F cell. Using an RVS, if it has a very low internal resistance, R_c, which in these examples would be the sum of the resistance of the wires plus the limiting resistor, the voltage drop ΔV is obtained using a simple voltage divider, given by the Equation (17), which can be easily measured, even if the no-load voltage of the source, E, or the current injected at the moment of connection, $i(t = 0)$, are low.
5. The method can be used by discharging the SC directly on a constant resistor R_c, the SC being at an initial voltage U_0, so that in the formulas shown, it would be sufficient to consider $E = 0$ V. In this case, the equipment needed to discharge the SC would be a simple low-value resistor, e.g., a piece of nichrome conductor. Its price would be considerably cheaper than that of a high current source or voltage source.

4. Results and Discussion

For the experimental tests, a Keithley™ 2440 SourceMeter (Keithley Instruments, Inc., Cleveland, OH, USA), configured as an ideal voltage source, was used, with an output voltage of 2.7 V set [54]. This piece of equipment can establish voltages at its external terminals between 5 μV and 42 V, with a measurement resolution of 1 μV. The connection cables between the source and the SC have an electrical resistance whose values are R_{w1} (positive) and R_{w2} (negative). The internal resistance of the SC will be denoted by R_0 (Figure 4).

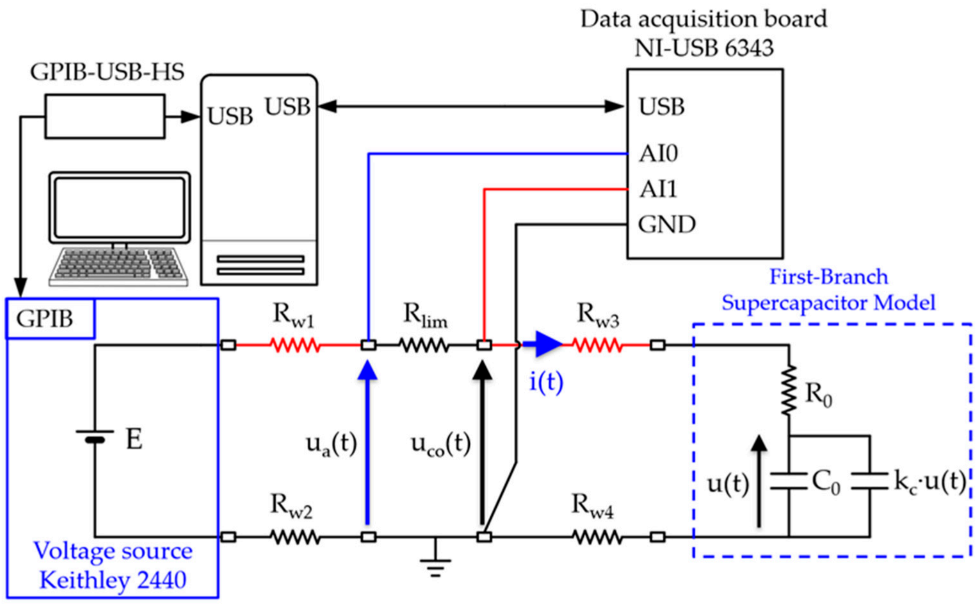

Figure 4. Connection of the measurement instruments.

As the source can supply a maximum current of 5 A, a series resistor, R_{lim}, of 496.7 mΩ was connected to limit the current set when the source is turned on. The resistances of the wires leading from the R_{lim} resistor to the SC were also measured; their values are R_{w3} (positive) and R_{w4} (negative). Given that the wires and connectors are not identical, the resistances R_{wj} (j = 1, 2, 3, 4) are different. To achieve the highest precision in measuring these low resistances, a 4-wire connection was employed. The values obtained are presented in Table 1, where the initial internal voltage of each cell, U_0, is also shown. In consideration of the diagram depicted in Figure 2, the resistance R_c used in the theoretical formulas described in Section 3 is equal to:

$$R_c = R_{w1} + R_{w2} + R_{lim}. \tag{38}$$

Table 1. Values of the wiring resistances in the tested SCs and initial voltage of the cells.

C_N [F]	R_{w1} [mΩ]	R_{w2} [mΩ]	R_{w3} [mΩ]	R_{w4} [mΩ]	U_0 [mV]
150	59.30	59.90	0	0	0
310	45.78	66.22	2.23	2.45	0
400	54.25	57.08	6.08	6.37	0
600	58.32	58.53	0	0	5

When the estimation methods described in Section 3 are applied, using the external voltage $u_{co}(t)$ (Figure 4), the value of the obtained resistance, R, can be expressed as the sum of the internal resistance of the SC, R_0, and the resistances of the cables, R_{w3} and R_{w4}. Subtracting those two latter from the value of R allows R_0 to be obtained.

The voltage $u_{co}(t)$ is measured by connecting its positive terminal to the analog input AI1 of a DA-NI-USB 6343™ data acquisition board, which has a resolution of 16 bits, and the negative terminal to its GND port. The resolution of the voltage measurement with the analog inputs is 0.152 mV and its accuracy is 1.52 µV [55]. The voltage $u_a(t)$ was measured at the analog input AI0 (Figure 4). The two analog inputs were configured in single-ended mode with an input range from −5 V to +5 V. The charging current, i(t), was obtained with the difference $u_a(t) - u_{co}(t)$ divided by the resistance R_{lim}. The chosen sampling period was 1 ms. The full instrumentation setup is shown in Figure 5.

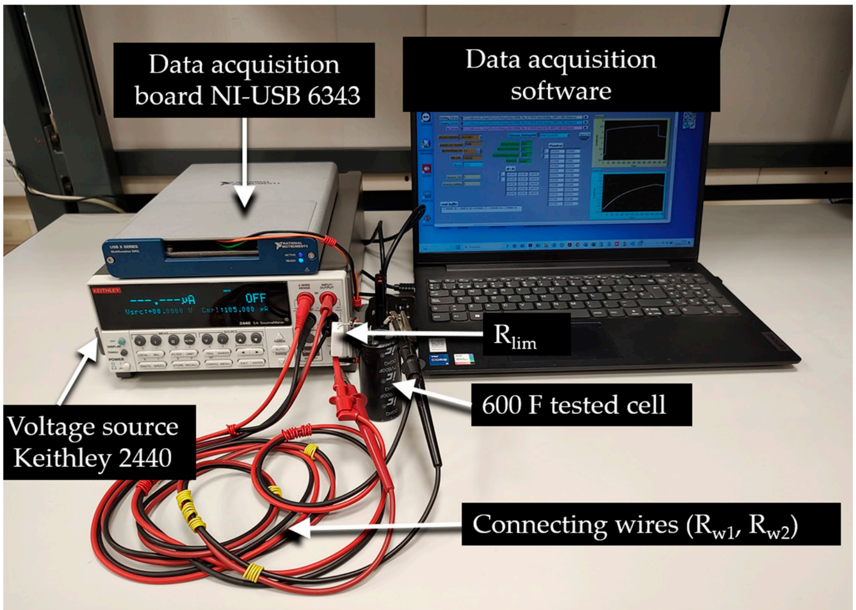

Figure 5. Full instrumentation used in the experimental tests.

Table 2 presents the most significant data for the SCs under consideration. These include the manufacturer, the rated capacitance, the rated resistance, and the rated voltage. Regarding the values in the datasheets provided by the manufacturers, it is necessary to clarify certain aspects. Firstly, the resistance and capacitance are obtained by assuming that the SC behaves as a constant capacitance RC circuit (Figure 1a), for which standardized IEC 62391-1 [56] and IEC 62391-2 [57] tests are used, without considering the leakage resistance R_L. Furthermore, it should be noted that there are certain unavoidable tolerances, inherent to the manufacturing process, which may result in discrepancies between the rated capacitance provided by the manufacturer and the real value measured. To ensure that the end user can work without encountering any issues, it is most common to indicate the rated value as the minimum obtained in the quality control process or to combine it with the typical and maximum values. When a manufacturer presents a single rated value, it signifies that the actual capacitance of the cell will be at least that value, but may be up to 20% higher, within the usual tolerances. The specifications may also appear, as in other electronic components, such as the rated value, C_N, together with the tolerances, e.g., (−5%, +10%). Similarly, the series resistance is typically presented by its maximum value, although the average or typical value may also be provided.

Table 2. Rated values of the tested SCs.

Manufacturer	C_{min} [F]	$C_{typical}$ [F]	C_{max} [F]	$R_{typical}$ [mΩ]	R_{max} [mΩ]	U_N [V]
Maxwell Technologies, San Diego, CA, USA.	**150**	165	180	4.0	6.5	3.0
Maxwell Technologies, San Diego, CA, USA.	**310**	-	-	-	2.2	2.7
Eaton, Cleveland, OH, USA	380	**400**	440	-	3.2	2.7
DGH, Knowles Corporation, Itasca, IL, USA	540	**600**	780	-	3.5	2.7

Table 2 presents the tolerances for capacitance and series resistance. The value designated as the rated capacitance is highlighted in bold. The temperature at which these values were measured is typically provided by the manufacturer: 20 °C or 25 °C. Figure 6 depicts a photograph of the cells tested, some of which have their connection cables already soldered.

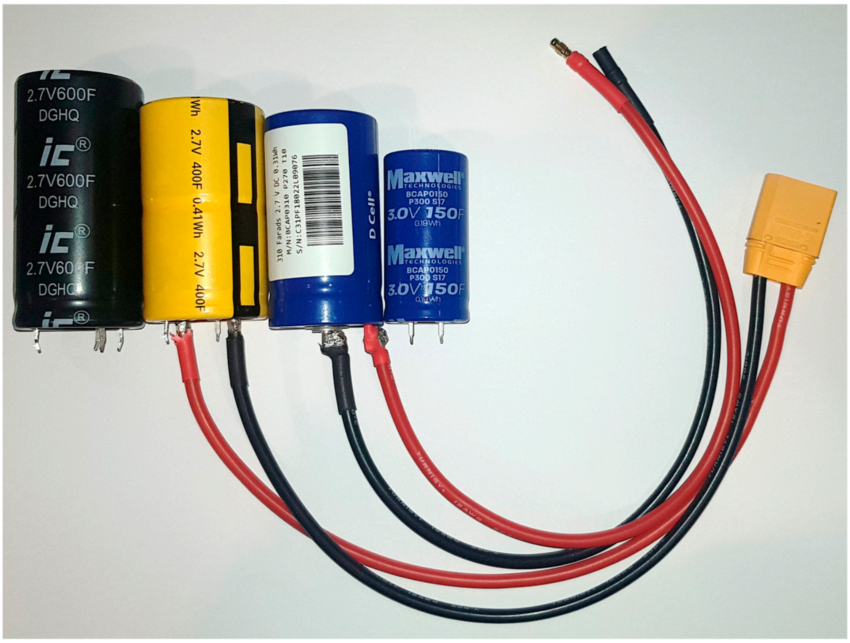

Figure 6. Tested SCs (capacitances of 150 F, 310 F, 400 F, and 600 F). For the 400 F and 310 F cells, the resistance value of the connection cables (R_{w3}, R_{w4}) has been considered.

Figure 7 illustrates the $u_{co}(t)$ voltage evolution, in the four cases, where the cells were connected to the RVS with E = 2.7 V. The SCs started with a zero initial voltage, except for the 600 F cell, which exhibited a residual voltage of 5 mV derived from previous tests. The source was activated 20 s after the beginning of data acquisition (19.2 s for the 400 F cell). The initial external voltage, u_{co1}, is dependent on the values of the resistances of the wires connecting the cell (R_{w1}, R_{w2}, R_{w3}, and R_{w4}). This is demonstrated in (17) and (38).

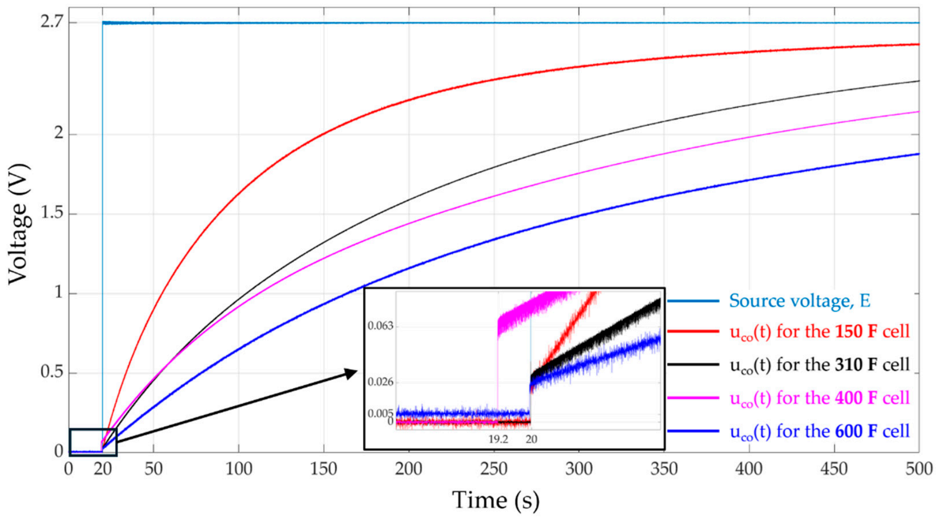

Figure 7. Measurement of the external voltage, $u_{co}(t)$, for the 150 F (red), 310 F (black), 400 F (magenta), and 600 F (blue) cells.

Figure 8 shows the charge current, i(t), in the four cases. The resistor R_{lim} has been selected with such a value that ensures the maximum current does not exceed 4.5 A, to provide a safety margin, given that the source is not capable of supplying more than 5 A. The lower the capacitance value, the faster the cell will charge and the faster the current will decrease.

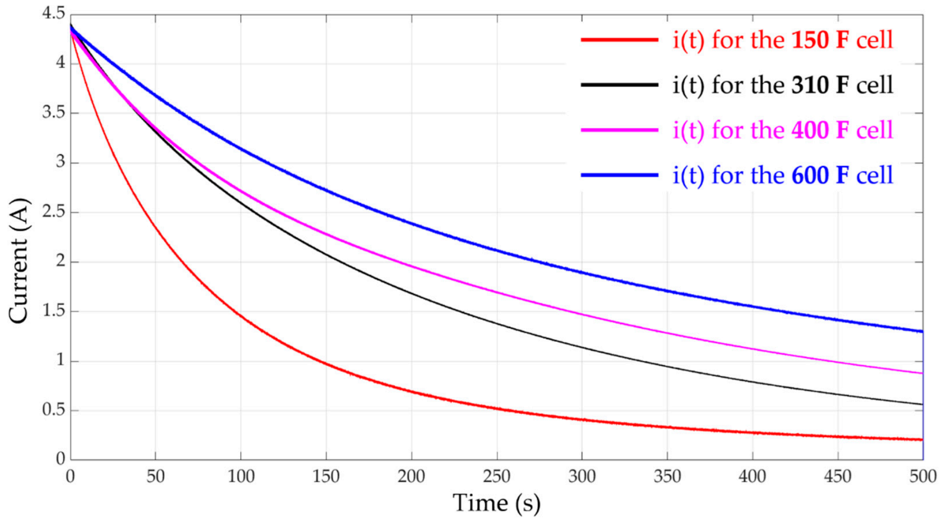

Figure 8. Measurement of the charging current, i(t), for the 150 F (red), 310 F (black), 400 F (magenta), and 600 F (blue) cells.

To calculate the parameters of the SCs under test, only the first 80 s of the data acquisition, measured from the moment of connection of the RVS, were taken, to avoid this way the secondary branch having time to charge. With these samples and the methods described above, the results shown in Table 3 were obtained. For the application of the 3PM, the time instants $t_1 = 0$, $t_2 = 40$, and $t_3 = 80$ s were considered. These measurements, taken just at those instants, were not averaged with the samples close to each other, so the values obtained with the LSM method will be more accurate. Even so, the results produced by both methods are very similar.

Table 3. Main branch values for all the SCs tested.

C_N [F]	Method	R_0 [mΩ]	C_0 [F]	k_c [F/V]
150	3PM LSM	4.268 4.195	101.575 101.343	21.323 21.476
310	3PM LSM	1.498 1.714	263.974 262.158	36.390 38.376
400	3PM LSM	2.173 1.458	269.304 268.362	65.425 65.017
600	3PM LSM	4.231 4.712	456.807 460.918	43.882 36.840

Table 4 shows the value of the Normalized Initial Capacitance, k_0, the estimated rated capacitance, $C_{N\text{-est}}$, calculated by expression (2), and the circuit time constant, τ, considered for the variable capacitance model, as defined in [31], whose theoretical expression is as follows:

$$\tau = R_{total} \cdot \left(C_0 + 2 \cdot k_c \cdot \left(U_0 + \frac{E - U_0}{e} \right) \right). \tag{39}$$

Table 4. Rated and normalized capacitances (C_N and k_0) and the time constant of the circuit.

C_N [F]	Method	$C_{N\text{-est}}$ [F]	k_0	τ [s]
150	3PM LSM	165.544 165.771	0.613 0.611	88.89 88.92
310	3PM LSM	362.228 365.773	0.729 0.717	206.76 208.14
400	3PM LSM	445.953 443.909	0.604 0.604	248.61 247.23
600	3PM LSM	575.288 560.387	0.794 0.822	336.23 330.36

In (39), R_{total} is the total resistance of the circuit (series connection of all that are present) and e is the Euler number.

The theoretical external voltage, $u_{co}(t)$, can be obtained from the estimated model parameters (Table 3) using Equations (4)–(7) and (10). It is also possible to analyze theoretically the behavior of the SC (one branch model with variable capacitance) considering the relationship between the external voltage, $u_{co}(t)$, and the current absorbed, i(t), according to the passive sign convention, as follows:

$$u_{co}(t) = R \cdot i(t) + u(t) = R \cdot i(t) + U_0 + \int_0^t \frac{i(t) \cdot dt}{C_0 + 2 \cdot k_c \cdot u(t)}. \quad (40)$$

In both ways, the external voltage can be calculated. The second option can be easily modeled with a simulation program. Figure 9 shows the block diagram created with Simulink^{TM} to reproduce the behavior of an SC considering only the main branch of variable capacitance, which will need the three parameters of the model (R, C_0, and k_c) and the value of the initial internal voltage, U_0. Connecting this block to a real voltage source (E, R_c) identical to the one used in the experimental tests, the theoretical value of the external voltage, $u_{co}(t)$, will be obtained.

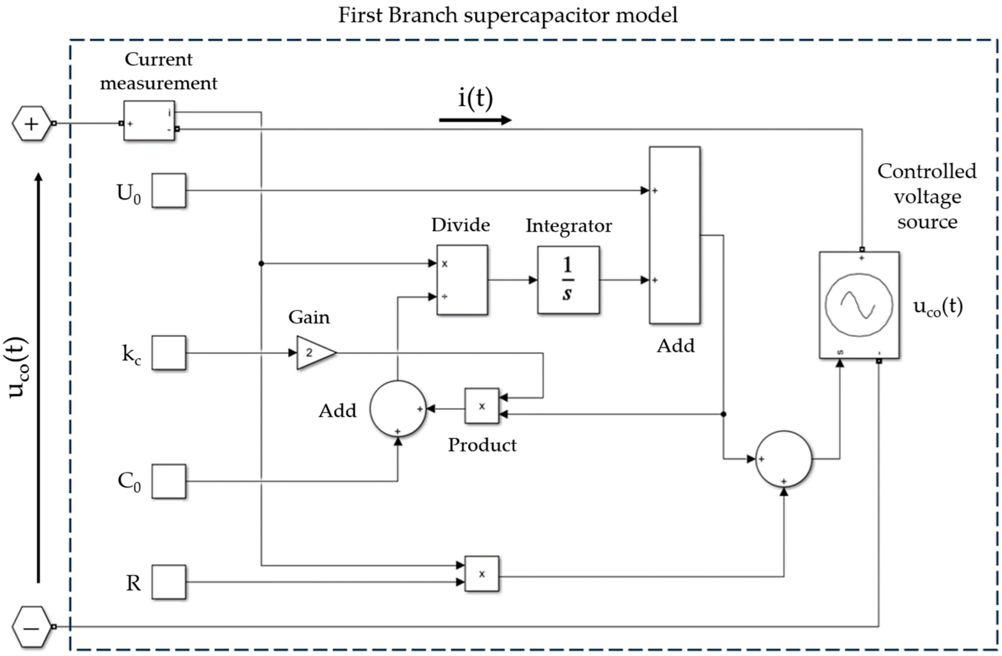

Figure 9. Block diagram created with Simulink to analyze theoretical cell behavior.

The theoretical external voltage, $u_{co}(t)$, was obtained using Simulink^{TM} software version R2021b, with the block diagram described in Figure 9 and graphically represented for the four cells tested alongside the actual recorded measurements, during the first 80 s, as shown in Figure 10. It can be observed that the theoretical and measured values of the external voltage are in perfect agreement. The model parameters chosen were those corresponding to the LSM method (Table 3).

Table 5 shows the values of the absolute error (minimum, maximum, and mean), calculated as the absolute value of the difference between the measured external voltage and the one estimated with the theoretical formulation. In this case, the absolute error was chosen because it is independent of time or SC voltage level, since it comes mainly from the A/D converter of the data acquisition board, while the relative error varies greatly depending on the instantaneous voltage of the cell. When this is close to zero, the relative error will be larger, being divided by a small value, and will decrease as the SC voltage increases. Its variance, σ, and the correlation coefficient R^2 of the fit are also shown. R^2 is, in all cases, very close to unity, again demonstrating the agreement between the calculations and the experimental measurements.

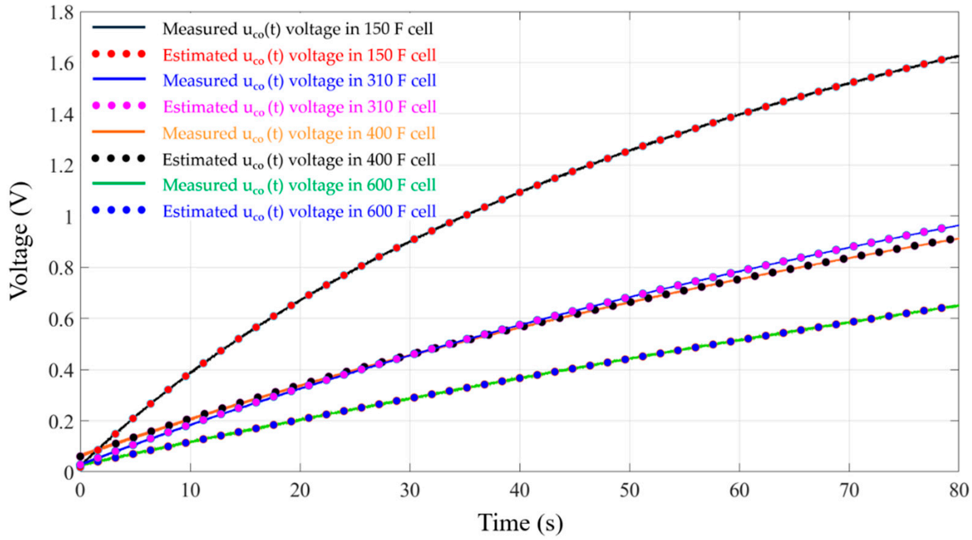

Figure 10. Voltage uco(t) measured and estimated from the values in Table 3 using the parameters obtained with the LSM method, for all the tested SCs.

Table 5. Main fit data. Errors and correlation coefficient.

C_N [F]	ε_{min} [mV]	ε_{mean} [mV]	ε_{max} [mV]	σ [mV^2]	Correlation Coefficient, R^2
150	2.572×10^{-6}	1.565	14.515	2.045	0.999977
310	30.532×10^{-6}	1.361	8.913	1.382	0.999955
400	1.392×10^{-6}	2.108	11.184	3.217	0.999872
600	35.268×10^{-6}	1.532	12.208	2.008	0.999866

5. Conclusions

The methods developed have been employed to analyze several SCs from different manufacturers, with capacities ranging from 150 F to 600 F. The variable capacity model parameters have been obtained and the experimentally recorded measurements have been compared with the theoretical curve, $u_{co}(t)$, which would be obtained with the calculated variables. The results show an almost perfect coincidence between both. The estimated values of series resistance and rated capacitances present a good agreement with the values specified by the manufacturers as well. The only differences with respect to the data given in the datasheets of the SCs are that, in the case of the 600 F cell, the measured value of internal resistance is 1 mΩ higher, while in the 400 F cell, the capacitance value measured in the test is 1% higher than the expected maximum value. However, it should be noted that the values provided by the manufacturers are measured considering the cells as an RC load of constant values, rather than considering the variable capacitance model, so it is reasonable to find slight discrepancies. The proposed methods have been demonstrated to be an alternative, and fairly accurate tool, for estimating the parameters of the main branch. They are capable of being calculated using a real voltage source or simply a constant resistance, in contrast to the current source that has been proposed by other authors to date.

Author Contributions: Conceptualization, J.F.P.; methodology, J.F.P. and M.F.Q.; software, M.F.Q., M.F.C. and E.E.Z.; validation, M.F.Q., G.A.O. and M.F.C.; formal analysis, J.F.P. and M.F.C.; investigation, M.F.Q., J.F.P. and G.A.O.; writing—original draft preparation, J.F.P.; writing—review and editing, E.E.Z., G.A.O., J.C.V. and M.F.C.; supervision, E.E.Z. and J.C.V.; project administration, J.C.V. and M.F.Q.; funding acquisition, J.C.V. and G.A.O. All authors have read and agreed to the published version of the manuscript.

Funding: This work has been partially funded by the Spanish Government, MCIN/AEI/FEDER, and the EU, under grants PID2021-122704OB-I00 and TED2021-131498B-I00.

Institutional Review Board Statement: Not applicable.

Informed Consent Statement: Not applicable.

Data Availability Statement: The original contributions presented in the study are included in the article, further inquiries can be directed to the corresponding author.

Conflicts of Interest: The authors declare no conflicts of interest.

Abbreviations

SC	Supercapacitor
C(u)	Variable capacitance [F]
C_0	Initial capacitance [F]
$C_1(u)$	Variable part of C(u) [F]
C_N	Rated capacitance [F]
R	Internal resistance of the SC [Ω]
R_{wi}	Electrical resistance of the wires [Ω]
U_N	Rated voltage [V]
k_0	Normalized Initial Capacitance (dimensionless)
u(t)	Internal voltage of SC [V]
U_0	Initial internal voltage of SC [V]
$u_{co}(t)$	External voltage of SC [V]
i(t)	Current [A]
RVS	Real constant voltage source
E	No-load voltage of the RVS [V]
R_c	Internal resistance of the RVS [Ω]
R_{lim}	Current-limiting resistor [Ω]
g(t)	Time function defined as $u(t) - E$ [V]
k_m	Constant measured in [V^{-1}]
k_n	Constant measured in [s^{-1}]
k_p	Constant (dimensionless)
k_1	Constant measured in volts
k_2	Constant (dimensionless)
k_3	Constant measured in [$V \cdot s^{-1}$]
α	Constant measured in seconds
β	Constant measured in seconds
γ	Constant measured in [$V \cdot s^{-1}$]
ε_{min}	Minimum error [mV]
ε_{mean}	Mean error [mV]
ε_{max}	Maximum error [mV]
σ	Standard deviation [mV^2]
R^2	Correlation coefficient of the fit
t	Time [s]
$W_0(x)$	Main branch of the Lambert-W function

References

1. Vandeginste, V. A Review of Fabrication Technologies for Carbon Electrode-Based Micro-Supercapacitors. *Appl. Sci.* **2022**, *12*, 862. [CrossRef]
2. Cabanas, M.F.; Duque, S.B.; González, J.D.; González, F.P.; Fernández, M.G. Preliminary Results of a Hybrid Thermoelectric Propulsion System for a Multirotor UAS with Active Rectifying, Electronic Throttle Control and Supercapacitors. *Appl. Sci.* **2021**, *11*, 7899. [CrossRef]
3. Lampasi, A.; Testa, R.; Gudala, B.; Terlizzi, C.; Pipolo, S.; Tenconi, S. Optimization of DC Energy Storage in Tokamak Poloidal Coils. *Appl. Sci.* **2024**, *14*, 8975. [CrossRef]

4. Burke, A.F.; Zhao, J. Development, Performance, and Vehicle Applications of High Energy Density Electrochemical Capacitors. *Appl. Sci.* **2022**, *12*, 1726. [CrossRef]
5. Carretero, A.; Real, S.; Araujo, A. Autonomous Active Tag Using Energy Harvesting Strategies. *Appl. Sci.* **2020**, *10*, 5260. [CrossRef]
6. Subasinghage, K.; Gunawardane, K. Supercapacitor-Assisted Energy Harvesting Systems. *Energies* **2024**, *17*, 3853. [CrossRef]
7. Detka, K.; Górecki, K. Selected Technologies of Electrochemical Energy Storage—A Review. *Energies* **2023**, *16*, 5034. [CrossRef]
8. Zhang, L.; Hu, X.; Wang, Z.; Sun, F.; Dorrell, D.G. A review of supercapacitor modeling, estimation, and applications: A control/management perspective. *Renew. Sustain. Energy Rev.* **2018**, *81*, 1868–1878. [CrossRef]
9. Pedrayes, J.F.; Melero, M.G.; Cano, J.M.; Norniella, J.G.; Duque, S.B.; Rojas, C.H.; Orcajo, G.A. Lambert W function based closed-form expressions of supercapacitor electrical variables in constant power applications. *Energy J.* **2021**, *218*, 119364. [CrossRef]
10. Marín-Coca, S.; Bifaretti, S.; Roibás-Millán, E.; Pindado, S. Mathematical modelling and performance analysis of supercapacitors with variable capacitance under constant power loads. In Proceedings of the 11th International Conference on Mathematical Modeling in Physical Sciences, Belgrade, Serbia, 5–8 September 2022; Volume 2872. [CrossRef]
11. Naresh, P.; Kishore, N.S.V.; Sravan Kumar, V.S. Design of Ultracapacitor based Energy Storage System for Constant Current and Constant Power Applications. In Proceedings of the 2022 IEEE International Conference on Power Electronics, Drives and Energy Systems (PEDES), Jaipur, India, 14–17 December 2022; pp. 1–5. [CrossRef]
12. Yang, H. Peukert's Law for Supercapacitors with Constant Power Loads: Applicability and Application. *IEEE Trans. Ind. Appl.* **2019**, *55*, 4064–4072. [CrossRef]
13. Pedrayes, J.F.; Melero, M.G.; Norniella, J.G.; Cano, J.M.; Cabanas, M.F.; Orcajo, G.A.; Rojas, C.H. A novel analytical solution for the calculation of temperature in supercapacitors operating at constant power. *Energy J.* **2019**, *188*, 116047. [CrossRef]
14. Victor Voicu, I.; Bode, F.; Abboud, W.; Louahlia, H.; Gualous, H.; Sandu, M.; Nastase, I. Experimental and Numerical Study for a Novel Arrangement of a SuperCapacitors Stack to Improve Heat Transfer. *Appl. Sci.* **2022**, *12*, 662. [CrossRef]
15. Pedrayes, J.F.; Melero, M.G.; Norniella, J.G.; Cabanas, M.F.; Orcajo, G.A.; González, A.S. Supercapacitors in Constant-Power Applications: Mathematical Analysis for the Calculation of Temperature. *Appl. Sci.* **2021**, *11*, 10153. [CrossRef]
16. Pedrayes, J.F.; Quintana, M.F.; Orcajo, G.A.; Zaldivar, E.E.V.; Melero, M.G.; Cabanas, M.F. Thermal Analysis of a Fast Charger for Public Service Electric Vehicles Based on Supercapacitors. *Batteries* **2024**, *10*, 128. [CrossRef]
17. Zhang, L.; Hu, X.; Wang, Z.; Sun, F.; Deng, J.; Dorrell, D.G. Multiobjective Optimal Sizing of Hybrid Energy Storage System for Electric Vehicles. *Trans. Veh. Technol.* **2018**, *67*, 1027–1035. [CrossRef]
18. Bolonne, S.R.A.; Chandima, D.P. Sizing an Energy System for Hybrid Li-Ion Battery-Supercapacitor RTG Cranes Based on State Machine Energy Controller. *IEEE Access* **2019**, *7*, 71209–71220. [CrossRef]
19. Pedrayes, J.F.; Melero, M.G.; Cano, J.M.; Norniella, J.G.; Orcajo, G.A.; Cabanas, M.F.; Rojas, C.H. Optimization of supercapacitor sizing for high-fluctuating power applications by means of an internal-voltage-based method. *Energy J.* **2019**, *183*, 504–513. [CrossRef]
20. Luta, D.N.; Raji, A.K. Optimal sizing of hybrid fuel cell-supercapacitor storage system for off-grid renewable applications. *Energy* **2019**, *166*, 530–540. [CrossRef]
21. Macias, A.; Kandidayeni, M.; Boulon, L.; Trovão, J.P. Fuel cell-supercapacitor topologies benchmark for a three-wheel electric vehicle powertrain. *Energy* **2021**, *224*, 120234. [CrossRef]
22. Pedrayes, J.F.; Melero, M.G.; Cabanas, M.F.; Quintana, M.F.; Orcajo, G.A.; González, A.S. Sizing Methodology of a Fast Charger for Public Service Electric Vehicles Based on Supercapacitors. *Appl. Sci.* **2023**, *13*, 5398. [CrossRef]
23. Yang, H.; Zhang, Y. Self-discharge analysis and characterization of supercapacitors for environmentally powered wireless sensor network applications. *J. Power Sources* **2011**, *196*, 8866–8873. [CrossRef]
24. Zubieta, L.; Bonert, R. Characterization of double-layer capacitors for power electronics applications. *Trans. Ind. Appl.* **2000**, *36*, 199–205. [CrossRef]
25. Devillers, N.; Jemei, S.; Péra, C.; Bienaimé, D.; Gustin, F. Review of characterization methods for supercapacitor modelling. *J. Power Sources* **2014**, *246*, 596–608. [CrossRef]
26. Grbovic, P.J.; Delarue, P.; Le Moigne, P.; Bartholomeus, P. Modeling and Control of the Ultracapacitor-Based Regenerative Controlled Electric Drives. *Trans. Ind. Electron.* **2011**, *58*, 3471–3484. [CrossRef]
27. Naseri, F.; Farjah, E.; Ghanbari, T.; Kazemi, Z.; Schaltz, E.; Schanen, J.-L. Online Parameter Estimation for Supercapacitor State-of-Energy and State-of-Health Determination in Vehicular Applications. *Trans. Ind. Electron.* **2020**, *67*, 7963–7972. [CrossRef]
28. Faranda, R. A new parameters identification procedure for simplified double layer capacitor two-branch model. *Electr. Power Syst. Res.* **2010**, *80*, 363–371. [CrossRef]
29. Nassef, A.M.; Fathy, A.; Rezk, H.; Yousri, D. Optimal parameter identification of supercapacitor model using bald eagle search optimization algorithm. *J. Energy Storage* **2022**, *50*, 104603. [CrossRef]
30. Marín-Coca, S.; Ostadrahimi, A.; Bifaretti, S.; Roibás-Millán, E.; Pindado, S. New Parameter Identification Method for Supercapacitor Model. *IEEE Access* **2023**, *11*, 21771–21782. [CrossRef]
31. Pedrayes, J.F.; Quintana, M.F.; Cabanas, M.F.; Melero, M.G.; Orcajo, G.A.; González, A.S. Non-Linear Analytical Model for the Study of Double-Layer Supercapacitors in Different Industrial Uses. *Appl. Sci.* **2023**, *13*, 6714. [CrossRef]

32. Staņa, Ģ.; Voitkāns, J.; Kroičs, K. Supercapacitor Constant-Current and Constant-Power Charging and Discharging Comparison under Equal Boundary Conditions for DC Microgrid Application. *Energies* **2023**, *16*, 4167. [CrossRef]
33. Reema, N.; Jagadan, G.; Sasidharan, N.; Shreelakshmi, M.P. Comparative Analysis of CC–CV/CC Charging and Charge Redistribution in Supercapacitors. In Proceedings of the 31st Australasian Universities Power Engineering Conference (AUPEC), Perth, Australia, 26–30 September 2021; pp. 1–5.
34. Li, H.; Zhang, X.; Peng, J.; He, J.; Huang, Z.; Wang, J. Cooperative CC–CV Charging of Supercapacitors Using Multicharger Systems. *IEEE Trans. Ind. Electron.* **2020**, *67*, 10497–10508. [CrossRef]
35. Zhang, X.; Liao, Y.; Li, H.; Liu, Y.; Zhang, R.; Meng, Z.; Peng, J.; Huang, Z. Consensus Control for CC–CV Charging of Supercapacitors. In Proceedings of the IEEE Energy Conversion Congress and Exposition (ECCE), Baltimore, MD, USA, 29 September–3 October 2019; pp. 2015–2020.
36. Ibrahim, T.; Stroe, D.; Kerekes, T.; Sera, D.; Spataru, S. An overview of supercapacitors for integrated PV—Energy storage panels. In Proceedings of the IEEE 19th International Power Electronics and Motion Control Conference (PEMC), Gliwice, Poland, 25–29 April 2021; pp. 828–835.
37. Milan, S.; Vračar, J.; Vračar, L. Different Ways to Charging Supercapacitor in WSN Using Solar Cells. In Proceedings of the 7th International Conference on Electrical, Electronic and Computing Engineering, IcETRAN, Palembang, Indonesia, 6–9 June 2022; pp. 28–29.
38. Sun, Y.; Yan, X. Recent advances in dual-functional devices integrating solar cells and supercapacitors. *Sol. RRL* **2017**, *1*, 1700002. [CrossRef]
39. Fernando, J.; Kularatna, N.; Silva, S.; Thotabaddadurage, S.S. Supercapacitor assisted surge absorber technique: High performance transient surge protectors for consumer electronics. *IEEE Power Electron. Mag.* **2022**, *9*, 48–60. [CrossRef]
40. Kularatna, N.; Subasinghage, K.; Gunawardane, K.; Jayananda, D.; Ariyarathna, T. Supercapacitor-Assisted Techniques and Supercapacitor-Assisted Loss Management Concept: New Design Approaches to Change the Roadmap of Power Conversion Systems. *Electronics* **2021**, *10*, 1697. [CrossRef]
41. Kularatna, N.; Fernando, J.; Pandey, A. Surge endurance capability testing of supercapacitor families. In Proceedings of the IECON 2010—36th Annual Conference on IEEE Industrial Electronics Society, Glendale, AZ, USA, 7–10 November 2010; pp. 1858–1863.
42. Silva Thotabaddadurage, S.U.; Kularatna, N.; Steyn-Ross, D.A. Optimization of Supercapacitor Assisted Surge Absorber (SCASA) Technique: A New Approach to Improve Surge Endurance Using Air-Gapped Ferrite Cores. *Energies* **2021**, *14*, 4337. [CrossRef]
43. Kularatna, N.; Gattuso, A.; Gurusinghe, N.; Jayasuriya, T.; Toit, J.D. Pre-stored supercapacitor energy as a solution for burst energy requirements in domestic in-line fast water heating systems. In Proceedings of the IECON 2014—40th Annual Conference of the IEEE Industrial Electronics Society, Dallas, TX, USA, 29 October–1 November 2014; pp. 3163–3167.
44. Gurusinghe, N.; Kularatna, N.; Charleston, S.A.; Fernando, J. System implementation aspects of supercapacitor based fast in-line water heating system. In Proceedings of the 2015 IEEE 24th International Symposium on Industrial Electronics (ISIE), Buzios, Brazil, 3–5 June 2015; pp. 1313–1317. [CrossRef]
45. Chavan, D.S.; Gadhwal, B.S.; Sankpal, J.; Siddhharth; Sahil, V.; Singh, A.; Dalal, M.K.; Priyanka. Ice melting from wind turbine blades using resistive heating. In Proceedings of the 2017 International Conference on Energy, Communication, Data Analytics and Soft Computing (ICECDS), Chennai, India, 1–2 August 2017; pp. 865–869. [CrossRef]
46. Grbovic, P.J. *Ultra-Capacitors in Power Conversion Systems: Applications, Analysis, and Design from Theory to Practice*; John Wiley & Sons: Hoboken, NJ, USA, 2013.
47. Maxwell Technologies. 310 F Datasheet. Available online: https://www.mouser.com/datasheet/2/257/bcseries_ds_1017105-2539864.pdf (accessed on 30 September 2024).
48. Maxwell Technologies. 150 F Datasheet. Available online: https://www.google.com.tw/url?sa=t&source=web&rct=j&opi=89978449&url=https://maxwell.com/wp-content/uploads/2021/08/3003112-EN.1_3V-150F-Datasheet.pdf&ved=2ahUKEwjN_M_ihraJAxXv1jQHHRhcKWoQFnoECBgQAQ&usg=AOvVaw0nMBzRmotK7PLqgYcyCxi9 (accessed on 30 September 2024).
49. Şahin, M.E.; Blaabjerg, F.; Sangwongwanich, A. Modelling of supercapacitors based on simplified equivalent circuit. *CPSS Trans. Power Electron. Appl.* **2021**, *6*, 31–39. [CrossRef]
50. Yasin, A.; Dhaouadi, R.; Mukhopadhyay, S. A Novel Supercapacitor Model Parameters Identification Method Using Metaheuristic Gradient-Based Optimization Algorithms. *Energies* **2024**, *17*, 1500. [CrossRef]
51. Jannif, N.I.; Kumar, R.R.; Mohammadi, A.; Cirrincione, G.; Cirrincione, M. Constrained Least-Squares Parameter Estimation for a Double Layer Capacitor. *Energies* **2023**, *16*, 4160. [CrossRef]
52. Corless, R.; Gonnet, G.H.; Hare, D.E.G.; Jeffrey, D.J.; Knuth, D.E. On the Lambert W function. *Adv. Comput. Math.* **1996**, *5*, 329–359. [CrossRef]
53. Mezo, I. *The Lambert W Function: Its Generalizations and Applications*, 1st ed.; Taylor & Francis Group: Abingdon, UK, 2022. [CrossRef]
54. Keithley Instruments, Inc. *User's Manual for Keithley Series 2400 SourceMeter®*; Document Number: 2400S-900-01 Rev. K/September 2011; Keithley Instruments, Inc.: Cleveland, OH, USA, 2011.
55. USB-6343 Specifications. Available online: https://www.ni.com/docs/en-US/bundle/usb-6343-specs/page/specs.html (accessed on 26 September 2024).

56. *IEC 62391-1*; International Standard, (part one), Edition 3.0. Fixed Electric Double-Layer Capacitors for Use in Electric and Electronic Equipment. International Electrotechnical Commission (IEC): Geneva, Switzerland, October 2022.
57. *IEC 62391-2*; International Standard, (part two), Edition 1.0b. Sectional Specfication—Electric Double Layer Capacitors for Power Application. International Electrotechnical Commission (IEC): Geneva, Switzerland, April 2006.